

On modeling global grain boundary energy functions

A. Morawiec

Institute of Metallurgy and Materials Science, Polish Academy of Sciences,
Kraków, Poland.

E-mail: nmmorawi@cyf-kr.edu.pl

Tel.: ++48-122952854, Fax: ++48-122952804

Abstract

Grain boundaries affect properties of polycrystalline materials. The influence of a boundary is largely determined by its energy. Grain boundary energy is often portrayed as a function of macroscopic boundary parameters representing grain misorientation and boundary plane inclination. In grain boundary simulation and modeling, many studies neglect structural multiplicity of boundaries, i.e., existence of metastable states, and focus on minimum energy. The minimum energy function restricted to constant misorientation should satisfy Herring's condition for interface stability. This requirement has been ignored in recent works on grain boundary energy functions. Example violations of the stability condition are shown. Moreover, a simple and natural procedure for constructing a continuous function satisfying the condition is described. Cusps in the energy as a function of boundary plane inclinations arise because of the imposition of the stability condition, and their locations and shapes result from properties of input data. An example of applying the procedure to simulated data is presented.

Keywords: Grain boundary energy; Anisotropy; Modeling; Misorientation; Grain boundary plane;

1 Introduction

Knowing grain boundary properties is important for modeling microstructures of polycrystalline materials. One of these properties is the boundary free energy. The practically feasible identification of boundary types is based on macroscopic boundary parameters (representing grain misorientations and boundary planes), and an energy function covering this parameter space is sought. Attempts are being made to determine such functions experimentally (e.g., [1–4]), but obtaining results with acceptable resolution and reliability is difficult. Another approach is to use atomic-scale simulations to compute energies of some pivotal boundaries and then use approximation methods to estimate energies of all other boundaries. It is well known from experiments and simulations that boundaries have multiple metastable structures. However, many studies on grain boundary simulation and modeling ignore structural multiplicity and deal with minimum energies. Recent years have seen a proliferation of publications on constructing global minimum energy functions based on data from simulations; see, e.g., [5–14]. Such functions have been used for polycrystal modeling, e.g., for simulation of grain growth under anisotropic conditions [15–18].

When grain misorientation is constant, the formal description of grain boundary energy as a function of boundary plane is analogous to that of surface energy. The minimum energy functions satisfy the condition for interface stability first precisely formulated by Herring [19]. This fact is well known, but has somehow been ignored in works on global grain boundary energy functions. Noncompliance with Herring’s condition is found in simulation data. In modeling of the energy function, noncompliance with the condition is also caused by an inappropriate model of energy cusps. For the consistency of boundary analysis with theory, it is important to recognize the nature of these contraventions and indicate ways to avoid them.

This paper recalls Herring’s interface stability condition and shows examples of its violation. Moreover, a simple procedure for constructing a continuous function that satisfies the condition is described. The first step of the procedure is to obtain a function that interpolates between data points. The interpolating function is then modified by imposing Herring’s condition on function’s restrictions to constant misorientations. This may lead to cusps in energy as a function of boundary plane even if the interpolating function does not have them. The procedure does not require entering cusp locations and there is no need for a cusp model. For illustration, results of application of the procedure to simulated data are presented. Examples below concern a single metal with cubic $m\bar{3}m$ symmetry, but key aspects of the paper apply to a broader class of materials.

2 Energy as a function of boundary plane inclination

The grain misorientation can be represented by a special orthogonal matrix, say M , and the boundary plane by a unit vector, say \mathbf{n} , normal to the plane with components given in the reference frame linked to the first crystal. The grain boundary free energy per unit area Γ is considered to be a function of M and \mathbf{n} . The function is assumed to be continuous, non-negative and bounded from above, with singularities where the derivative of the function does not exist. The singularities are usually referred to as energy cusps when shown in sections through Γ . It is also assumed that Γ decreases with decreasing misorientation angle when the latter is smaller than a certain limiting value, and Γ equals zero at zero misorientation angle.

Let the grain misorientation be fixed at M , and let the variable vector \mathbf{n} cover the sphere. The focus below will be on the function γ defined as $\gamma(\mathbf{n}) = \Gamma(M, \mathbf{n})$. Physically, the case with fixed misorientation can be viewed as a crystal embedded inside another crystal. The configuration is similar to that considered with respect to the equilibrium shape of a crystal immersed in another medium. Knowing γ , one can draw and analyze its spherical plot, i.e., the Wulff plot.

Example Wulff plots are shown in Fig. 1. These are sections through the closed-form energy function described in the paper of Bulatov et al. [7]. The function is based on atomic-scale simulations of Olmsted et al. [20] and a-priori selected locations of cusps. The function is constructed by what is called ‘hierarchical interpolation’, but is actually a fitting, and the angular dependence of energy in the presence of a cusp follows the model of Wolf [21]. Fig. 1 and all other examples below are based on data for Ni taken from [20] and [7].

2.1 H-convexity of energy function

When energy functions are constructed by approximating simulated data, atomistic and continuum models are intertwined. In the continuum model, the boundary energy is understood to be the excess free energy associated with the presence of the boundary per unit area. The question arises about the nature of the energy obtained in simulations. Costs of computing grain boundary energy from first principles is currently too high for any extensive coverage of the five-dimensional parameter space. Therefore, simplified computational schemes are used. Most estimations of grain boundary energy rely on athermal molecular dynamics simulations at 0K. Typical determination of the boundary energy involves multiple (macroscopically equivalent) initial atomic configurations [9–12, 20]. For each initial configuration, the simulation software searches for the configuration with minimum energy.

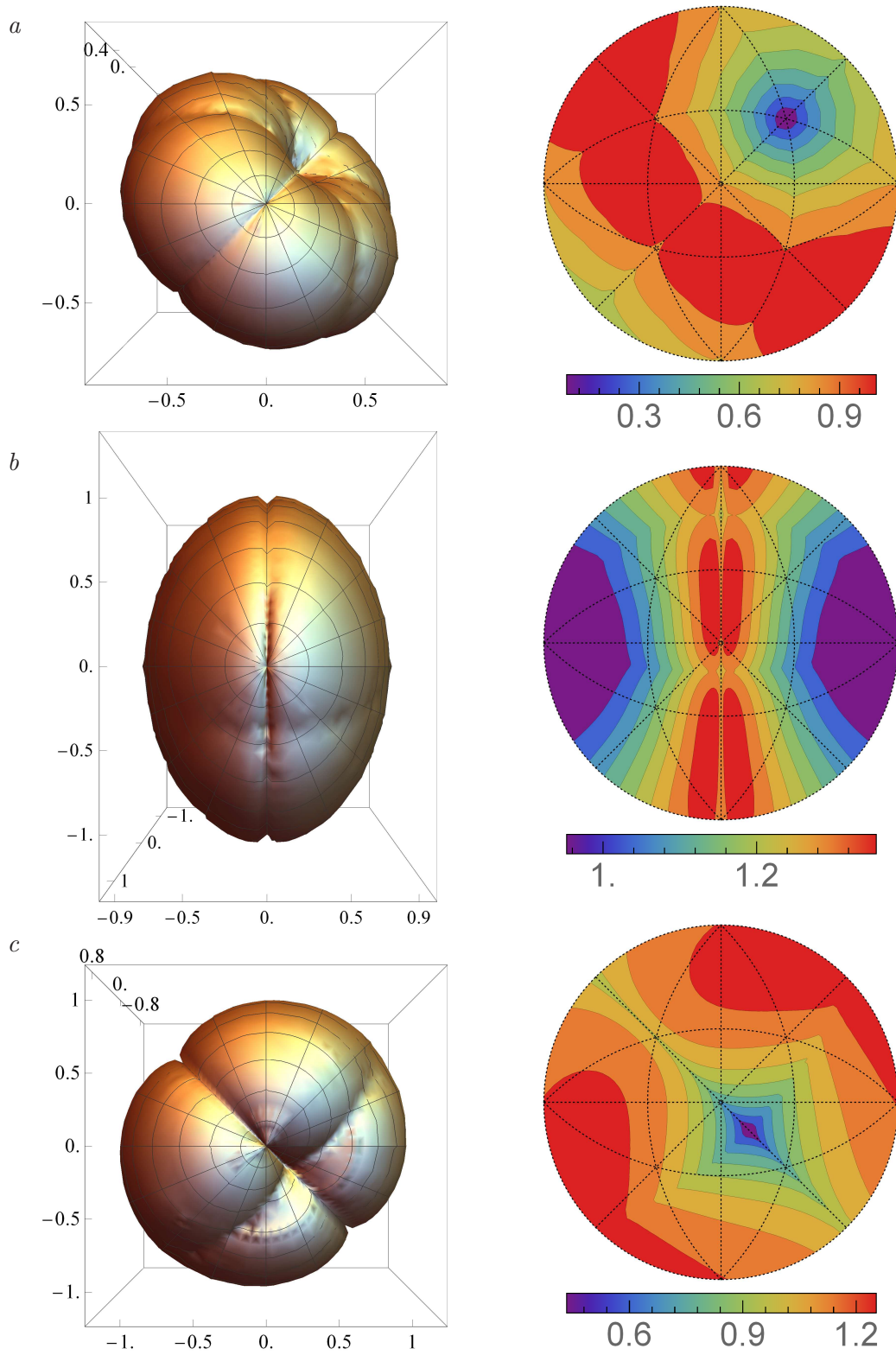


Figure 1: Wulff plots and their stereographic projections for Ni and the misorientations $\Sigma 3$, i.e., 60° rotation about $[111]$ (a), $\Sigma 5$, i.e., $\arccos(4/5) \approx 36.87^\circ$ rotation about $[100]$ (b) and $\Sigma 11$, i.e., $\arccos(7/11) \approx 50.48^\circ$ rotation about $[110]$ (c) based on the energy function of Bulatov et al. [7]. The stereographic projections shown here and in Fig. 6 were drawn using the program of Głowiński [22]. The energy unit is J/m^2 .

This minimum energy usually varies with the initial configuration, meaning that energy minima are local and boundary states are metastable. In the end, the lowest of the energies obtained from all tested initial configurations is taken as the actual energy of the boundary under consideration. Thus, in such simulations, the search is for ‘global minima’ of the energy. Such minima correspond to equilibrium states. The equilibrium states are rarely achieved in real materials and are difficult to reach in simulations, but their energies are unique, while those of metastable states can spread over wide ranges.

It follows from the above that if a given value of boundary energy results from simulation aimed at finding minimum-energy configurations, it should not be possible to assign any lower energy to this boundary. However, this rule is not always met. This can be demonstrated using standard Herring’s [19] analysis of Wulff plots or its version based on $1/\gamma$ -plots [23]. The short formulation of the second approach is that for the boundary normal to \mathbf{n} to be in equilibrium, the point $\mathbf{n}/\gamma(\mathbf{n})$ must lie on the convex hull of the $1/\gamma$ -plot. A function on the unit sphere satisfying the above (Herring) condition will be called h-convex, and a pentavariate function Γ will be referred to as h-convex if all its restrictions γ for misorientations held constant are h-convex.

Example non-convexity of a $1/\gamma$ -plot obtained based on the data set from [20] is shown in Fig. 2. Deviations from convexity are small, but quite common. In the case of Ni and $M = \Sigma 3$, after taking into account symmetry [24, 25], the number of distinct data points is 566, whereas the convex hull of the $1/\gamma$ -plot has only 44 vertices.

The lack of h-convexity means that some energies are too high. In minimization of the crystal surface energy within the continuum model, such high energies imply missing surface orientations, i.e., the corresponding regions of the Wulff plot are in a sense ‘passive’, and “‘passive’ regions of the Wulff plot ... have no significance” [26]. The same applies to grain boundary energies. The only characteristic energy of a boundary is defined by the convex hull of the $1/\gamma$ -plot. The passive regions of the Wulff plot correspond to Herring’s ‘hill-and-valley’ structures [19]. In the case of boundaries, planes in passive regions are unstable and they facet.

On the other hand, simulated boundaries in passive regions are stable against faceting. By using molecular statics at zero temperature, faceting is avoided, and the result of the computation is assumed to represent energy of the boundary plane selected at the outset. In other words, the idea is that the simulation result is the lowest energy of non-faceted boundary with the plane matching the assumed macroscopic model. However, by the nature of atomic simulations, the boundary is not flat, and it has a non-zero thickness, i.e., it cannot

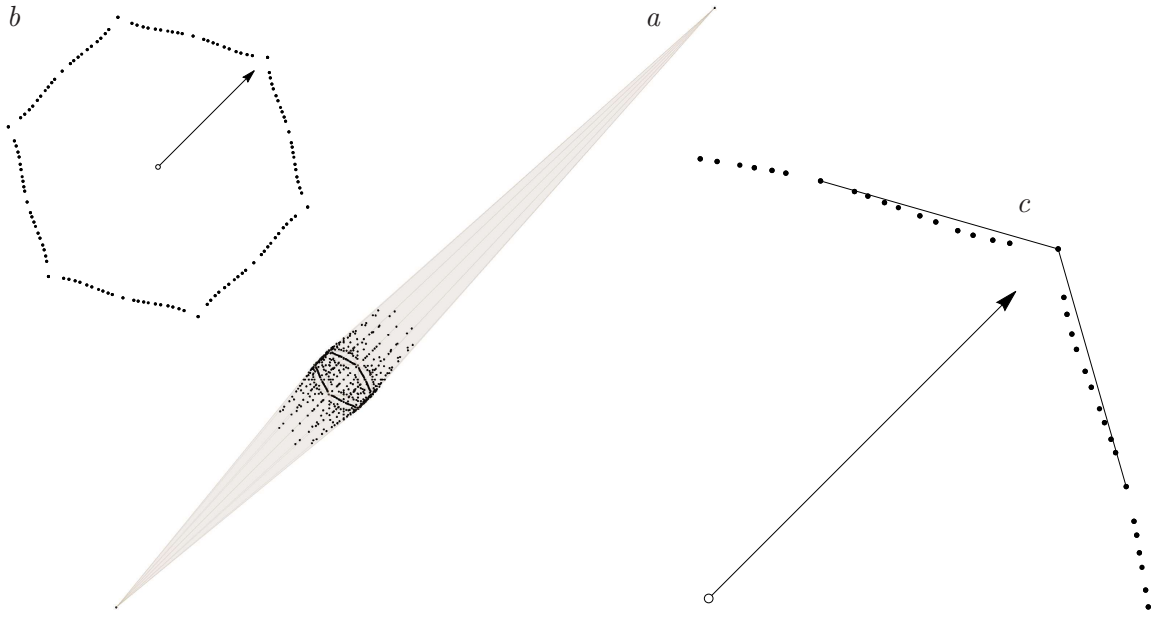


Figure 2: The $1/\gamma$ -plot based on data of Olmsted et al. [20] for Ni and the misorientation $\Sigma 3$ (*a*). To guide the eye, the convex hull of the point set is marked. The most distant vertices correspond to $\pm(111)$ planes. Section of the $1/\gamma$ -plot perpendicular to $[111]$ and a part of it demonstrating that the plot is not convex are in *b* and *c*, respectively. The vector shown in *b* and *c* indicates $(11\bar{2})$ plane and its magnitude is $1/(J/m^2)$.

match the plane exactly. The magnitudes of deviations of the true structure from the ideal flat zero-thickness macroscopic archetype vary from case to case, and there are no definite limits on the allowed deviations. There is no clear-cut distinction between faceted and non-faceted forms of a boundary, as boundary facets may vary in size from micro- and nano-scale facets observed in electron microscopes (e.g. [27]) to ‘atomistic’ facets of Brokman et al. [28] with facet recognition based on the observed arrangement of atoms within the structural unit of the boundary. The results obtained from simulations incorporate the energies of facet edges and corners and their interactions. The key point is that this energy depends on the density of the edges and corners. The density-dependent energy is not unique and it is not specific to the boundary defined by macroscopic parameters. What is specific and unique is the limiting value to which the energy tends as the facet size increases. This lower bound to energies the boundary may have is the energy of the equilibrium configuration.

Similarly, continuous functions approximating simulated data sets containing global energy minima for selected macroscopic boundary types are expected to represent the energies of the equilibrium states. The continuous function of Bulatov et al. [7] inherits non-convexities of the $1/\gamma$ -plots from the data on which it is based, but this function has an additional reason for them to occur. It is the model of the energy cusp.

3 Cusp model

The shape of energy near cusps is frequently modeled by the Read-Shockley function $E_0 \theta (A_1 - \ln \theta)$, where θ denotes the angle of misorientation from the position of the cusp, and E_0 and A_1 are parameters [29]. Closely related is the Read-Shockley-Wolf (RSW) model. In a slightly simplified form, with a , b and g_0 denoting model parameters, it is given by $\gamma_{RSW}(\theta) = g_0 + b \sin \theta (1 - a \ln \sin \theta)$ [21].¹ In [7–12], the use of the RSW model is extended beyond misorientation angles, and it affects arbitrary cusps in Γ including those with respect to inclination parameters, i.e., cusps in γ functions at fixed misorientations. It is easy to see, however, that γ_{RSW} has an infinite slope at the cusp, and in effect, the $1/\gamma$ -plot near an RSW-modeled cusp is not convex; see Figs. 3 and 4. Therefore, γ_{RSW} is not suitable for modeling cusps in γ functions.

The question is what is the formula for a cusp in γ when it arises due to an edge of flat faces of the $1/\gamma$ -plot. It can be easily obtained by considering a two-dimensional case. Let

¹Assuming small θ , Read and Shockley approximated $2 \sin(\theta/2)$ by θ [29]. In Wolf’s paper [21], $2 \sin(\theta/2)$ is replaced by $\sin \theta$. This gives zero slope at $\theta = \pi/2$ and simplifies the use of γ_{RSW} over the range $0 \leq \theta \leq \pi/2$.

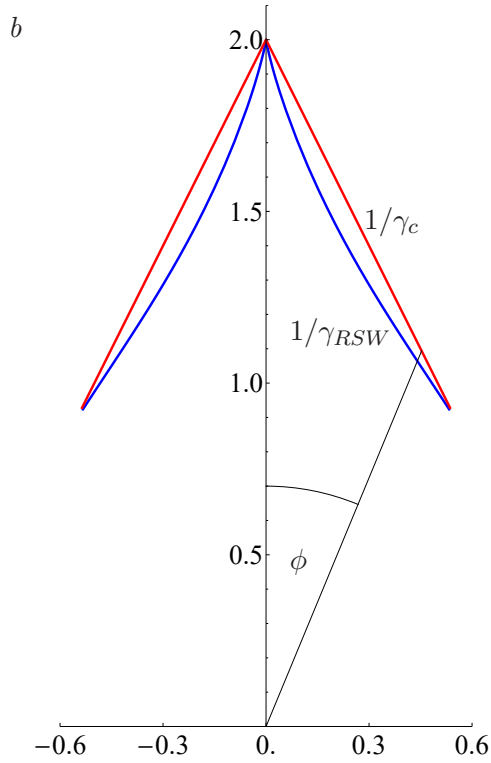
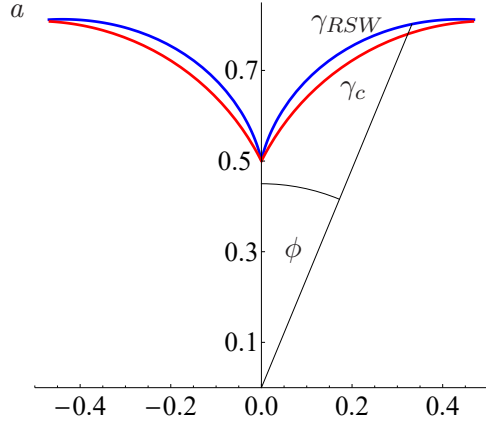


Figure 3: Parts of Wulff plots $\gamma_{RSW}(|\phi|) \times (\sin \phi, \cos \phi)$ (blue) and $\gamma_c(|\phi|) \times (\sin \phi, \cos \phi)$ (red) (a) and corresponding $1/\gamma$ -plots (b) for $a = 0.5$, $b = 0.65$, $g_0 = 0.5$, $g_{\pi/2} = 1$, and ϕ in the range from $-\pi/6$ to $\pi/6$. The angle between the branches of γ_{RSW} at the cusp is 0, and the same applies to the branches of $1/\gamma_{RSW}$. The angle between the branches of γ_c at the cusp is $2 \arctan(g_0/g_{\pi/2})$, and the same angle is formed by the branches of $1/\gamma_c$.

\mathbf{n}_c be the direction at which two faces of $1/\gamma$ -plot meet, let the vector \mathbf{n} vary in a fixed plane containing \mathbf{n}_c , and let ϕ ($0 \leq \phi \leq \pi/2$) denote the angle between \mathbf{n}_c and \mathbf{n} . Then the energy function has the form

$$\gamma_c(\phi) = g_0 \cos \phi + g_{\pi/2} \sin \phi, \quad (1)$$

where g_0 (> 0) is the energy at the cusp, and the derivative of γ_c at the cusp is $g_{\pi/2}$ (> 0), i.e., the slope is finite (Fig. 3). With $0 \leq \phi \leq \pi/2$, the curve $\gamma_c(\phi)$ ($\sin \phi, \cos \phi$) (seen as a fragment of two-dimensional Wulff plot) is a part of the circle centered at $(g_{\pi/2}, g_0)/2$ and passing through the points $(0, 0)$, $(0, g_0)$ and $(g_{\pi/2}, 0)$; cf. [19]. By definition of γ_c , the curve $(\sin \phi, \cos \phi)/\gamma_c(\phi)$ (seen as a fragment of two-dimensional $1/\gamma$ -plot) is a segment of a straight line through $(0, 1/g_0)$ and $(1/g_{\pi/2}, 0)$.

4 H-convex energy model

The essence of boundary energy modeling is to construct a global energy function based on discrete data. The function, satisfying conditions listed in section 2, is expected to be not only close to the simulated data but also h-convex.

Let γ_0 be a function on the unit sphere. If γ_0 violates the condition of h-convexity, it can be modified so the condition is satisfied: each point inside the convex hull of the $1/\gamma_0$ -plot is replaced by that on the convex hull. In other words, given the function γ_0 , one must first obtain the $1/\gamma_0$ -plot and determine its convex hull, and the modified function is given by $\gamma(\mathbf{n}) = 1/q(\mathbf{n})$, where $q(\mathbf{n})$ is the distance from the origin of the reference frame to the hull in the direction \mathbf{n} . This modification will be called h-convexification. Note that to compute the value of the h-convex γ for a single direction \mathbf{n} , it is necessary to know γ_0 over the entire sphere. The important point is that the new h-convex function γ may have singularities even if γ_0 is differentiable. Singularities will arise when the convex hull of the $1/\gamma_0$ -plot has vertices and/or edges; the function q is not differentiable at directions corresponding to such points, and this means that γ is also singular at these directions.

In practice, it is convenient to h-convexify γ_0 using a discrete set of directions. One needs to generate a sufficient number N_P of auxiliary vectors \mathbf{n}_p on the unit sphere, get the set P of points $\mathbf{n}_p/\gamma_0(\mathbf{n}_p)$ ($p = 1, 2, \dots, N_P$), and determine its convex hull, i.e., the convex polyhedron (seen as a union of convex polygons [30]) that encloses P and whose vertices are in P .² Natural candidates for the vectors \mathbf{n}_p are normals to low-index lattice planes.

²The distance from the origin to a point on a face of the polyhedron can be seen as a linear interpolation over distances to the vertices of that face. H-convexification of the function γ_0 can be seen as *linear*

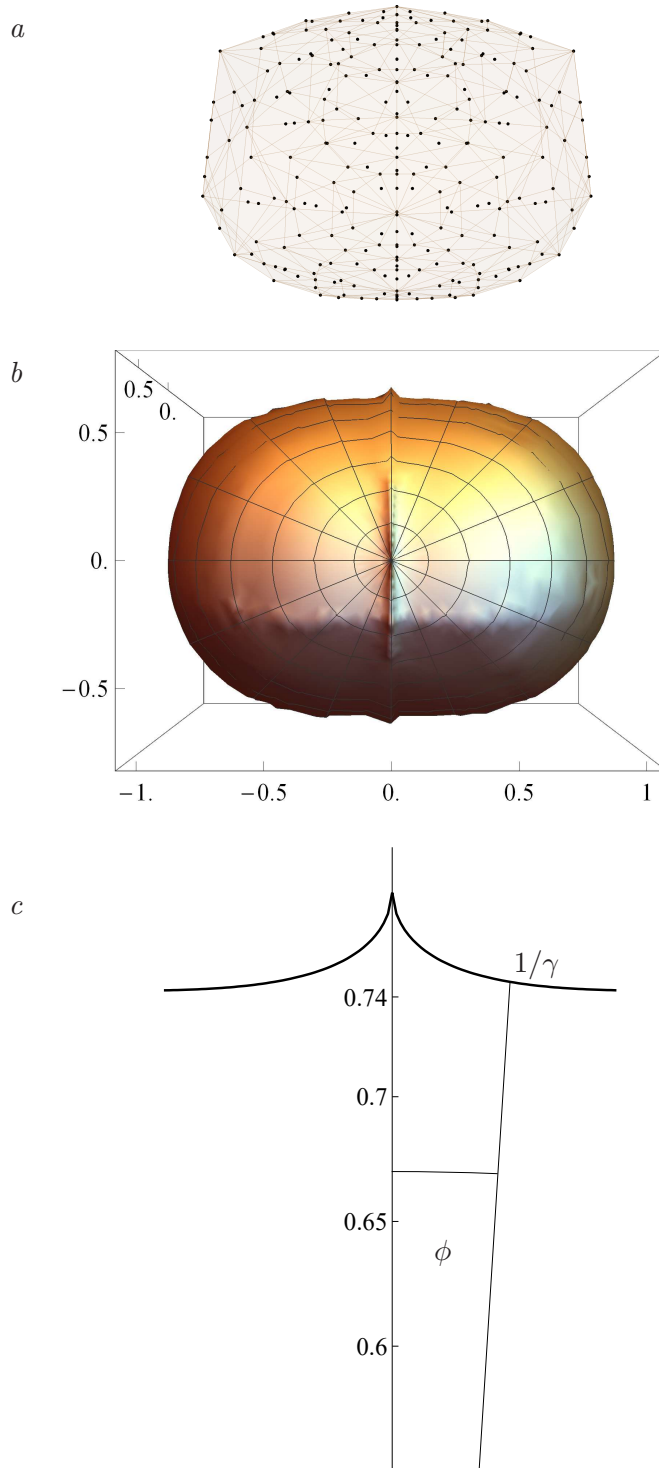


Figure 4: (a) The $1/\gamma$ -plot based on data of Olmsted et al. [20] for Ni and the misorientation $\Sigma 5$. (b) The corresponding $1/\gamma$ -plot obtained from Γ of Bulatov et al. [7]. It has a ridge at directions perpendicular to the misorientation axis $[100]$. (c) Section through the plot shown in (b) perpendicular to the ridge. It illustrates non-convexity of $1/\gamma$ -plot. The energy unit is J/m^2 .

Clearly, with this approach, presence of singularities in the resulting h-convex function is certain, and cusps have shapes described by eq.(1).

Let h-convexification of a pentavariate function Γ_0 defined on the entire space of macroscopic parameters mean h-convexification of its restrictions to functions γ_0 for constant misorientations. A simple and natural method to construct a proper energy function Γ is by h-convexifying a preliminary function that well approximates the discrete simulation data. So the first step is to devise a function Γ_0 that will give an approximate energy at any point \mathbf{B} based on known energies at points \mathbf{B}^κ ($\kappa = 1, 2, \dots, K$). One may ask why introduce an approximation function Γ_0 instead of directly h-convexifying the discrete data set consisting of known energies at points \mathbf{B}^κ . The reason is that for some misorientations the number of known energies is small, and for most (or precisely ‘for all except for finitely many’) misorientations there are no data points at all.

One way to get Γ_0 is by interpolation. It is clear that in order to estimate Γ at a single point, say $\mathbf{B} = (M, \mathbf{n})$, one must first calculate the interpolated values Γ_0 for N_P points $\mathbf{B}_p = (M, \mathbf{n}_p)$. The number N_P affects the computation time, but if it is large enough, it has no practical effect on the shape of Γ . The scheme for computing the value of h-convex Γ for a given \mathbf{B} is outlined as Algorithm I below.

H-convexification may cause singularities with respect to boundary plane inclination. There is a question if the function Γ resulting from h-convexification of Γ_0 differentiable with respect to misorientation parameters will also have this property. There is no simple answer, as in cases other than ‘twists’ around normals to fixed planes, a change of misorientation implies a change in (at least one of) boundary planes.

It is worth making a digression on taking into account supplementary information on boundary energy. A simple way to do this is by appending the simulated data with extra points carrying the information. It is natural to add the point with zero energy at the configuration \mathbf{B}^0 with zero misorientation angle. Similarly, if there is little data for low-angle boundaries, one may want to include a low-angle boundary model by appending extra points with energies based on the model to the initial data set. Merging datasets is a natural method for combining boundary data from different sources (e.g., simulation and experimental data).

interpolation over extreme points of the convex hull of the point set P .

Input: Parameters of the boundary \mathbf{B} whose energy is to be calculated

Input: List of K boundaries \mathbf{B}^κ and corresponding energies Γ_0^κ

Input: Subsidiary parameters N_P and u

```

/* Initialization */
Decompose  $\mathbf{B}$  into  $(M, \mathbf{n})$ 
Generate  $N_P$  auxiliary directions  $\mathbf{n}_p$ 

/* Interpolation between irregularly spaced data points */
/* For demonstration purposes, inverse distance weighting is used */
Define the distance function  $\tilde{d}$ 
for  $p = 1, 2, \dots, N_P$  do
     $\mathbf{B}_p = (M, \mathbf{n}_p)$ 
    for  $\kappa = 1, 2, \dots, K$  do
         $d_\kappa = \tilde{d}(\mathbf{B}_p, \mathbf{B}^\kappa)$ 
         $\gamma_0(\mathbf{n}_p) = \sum_\kappa d_\kappa^{-u} \Gamma_0^\kappa / \sum_\kappa d_\kappa^{-u}$  /*  $= \Gamma_0(\mathbf{B}_p)$  */
/* Determination of the point set  $P$  */
for  $p = 1, 2, \dots, N_P$  do
     $\mathbf{x}_p = \mathbf{n}_p / \gamma_0(\mathbf{n}_p)$ 
/* Determination of the convex hull of  $P$  */
Call routine that determines the smallest convex polyhedron enclosing all points  $\mathbf{x}_p$ 
/* Final step */
 $\mathbf{x}$  = the point of intersection of the line  $\lambda \mathbf{n}$  ( $\lambda > 0$ ) with the polyhedron
 $q(\mathbf{n}) = |\mathbf{x}|$ 
 $\gamma(\mathbf{n}) = 1/q(\mathbf{n})$ 

Result: Value of the h-convexified function  $\Gamma$  at  $\mathbf{B}$ :  $\Gamma(\mathbf{B}) = \gamma(\mathbf{n})$ 

```

Algorithm I: Sketch of the subroutine for determining h-convex Γ for arbitrary boundary \mathbf{B} based on energies Γ_0^κ for a discrete set of boundaries \mathbf{B}^κ .

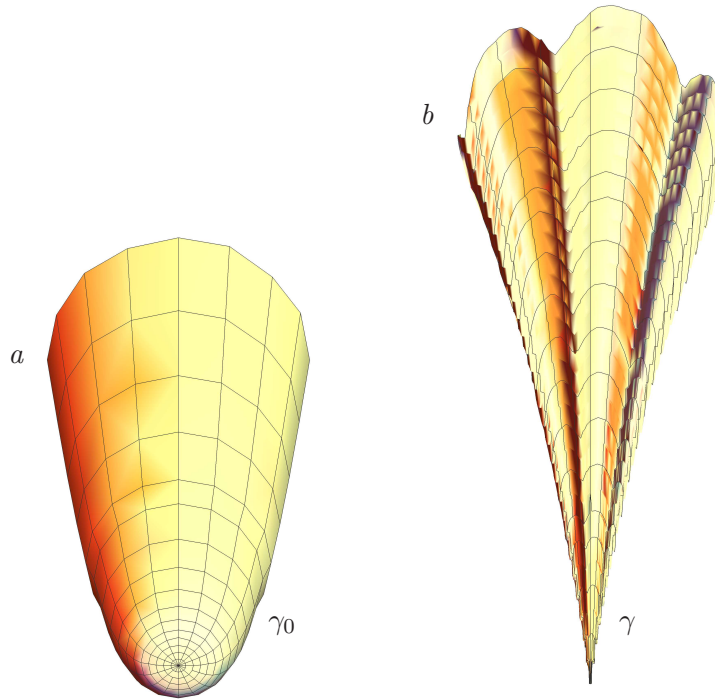


Figure 5: The dips in γ -plots at $[111]$ for $\Sigma 3$ misorientation modeled by the interpolating function γ_0 obtained by inverse distance weighting of data from $[20]$ (*a*) and γ obtained by h-convexification of γ_0 (*b*). The maximal deviation of shown directions from $[111]$ is 3° . The function γ_0 is differentiable whereas γ lacks differentiability at $[111]$ (i.e., at the projectile point of the ‘arrowhead’) and along edges of the ‘arrowhead’.

4.1 Example

H-convexification will be illustrated on data of Olmsted et al. [20]. The dataset contains energies Γ_0^κ for $K = 388$ boundary types \mathbf{B}^κ ($\kappa = 1, 2, \dots, K$). The set was appended with the point of zero energy at \mathbf{B}^0 . The preliminary function Γ_0 was constructed by interpolation. A simple method for interpolating between irregularly spaced data points in metric spaces is Shepard’s inverse distance weighting [31]. Let \tilde{d} be a symmetry-invariant distance function on the boundary space [32]. To get the value of Γ_0 at \mathbf{B} one needs the distances $d_\kappa = \tilde{d}(\mathbf{B}, \mathbf{B}^\kappa)$ of \mathbf{B} to data points \mathbf{B}^κ . The interpolated value $\Gamma_0(\mathbf{B})$ is the arithmetic average of Γ_0^κ weighted by d_κ^{-u} ($u > 0$). Unless stated otherwise, the parameter u was set to 4, and boundary distances were computed using the function \tilde{D}_M defined in [24].³ The interpolating function Γ_0 calculated in this way is not only continuous but also differentiable⁴ (Fig. 5a). The function Γ_0 obtained from data of Olmsted et al. [20] was not h-convex. It was h-convexified using $N_P \approx 2.4 \times 10^3$ auxiliary directions. If the direction \mathbf{n}_p was used, so were the directions symmetrically equivalent to it. Convex hulls were calculated using the code of O’Rourke [30, 33]. Example sections through the interpolating function Γ_0 and the function Γ resulting from h-convexification of Γ_0 are shown in Fig. 6. Since the computation of Γ is based on a finite number of points, individual $1/\gamma$ -plots are polyhedra, and in effect, Γ has multiple singularities at constant misorientations. Due to the high value of N_P , most of them are unnoticeable, but some are clearly visible (Fig. 5b).

Clearly, the shape of the Γ function is influenced by the choice of the interpolation method, but this effect is mitigated by h-convexification. This can be observed by testing Γ_0 and Γ for different values the u parameter and different distance functions. When u is small, the interpolating function is strongly attracted to the arithmetic mean $\sum_\kappa \Gamma_0^\kappa / K$ and exhibits large oscillations. When u is large, results of inverse distance weighting are close to those of the nearest-neighbor interpolation and this dulls extrema. Example functions for $u = 3$, $u = 4$ and for the distance functions \tilde{D}_M [24] and \tilde{D}_a [34] are compared in Fig. 7. This figure also shows that the character of the function Γ resulting from h-convexification can differ considerably from that of the preliminary Γ_0 . Sections through h-convex Γ for fixed misorientation are simple compared to those through the interpolating function Γ_0 , and edges and vertices of convex hulls of $1/\gamma$ -plots give rise to singularities with respect to boundary inclination parameters. This, however, does not apply to misorienta-

³Since \mathbf{B}^0 has multiple representations (I, \mathbf{n}) , where I is the identity matrix and \mathbf{n} is an arbitrary unit vector, the distance from \mathbf{B} to \mathbf{B}^0 is $d_0 = \min_{\mathbf{n}} \tilde{d}(\mathbf{B}, (I, \mathbf{n}))$. For distance functions denoted in [32] by a capital letter D , d_0 is the misorientation angle of \mathbf{B} times a constant factor.

⁴With $u > 1$, first derivatives of Γ_0 at data points $\mathbf{B} = \mathbf{B}^\kappa$ are zero.

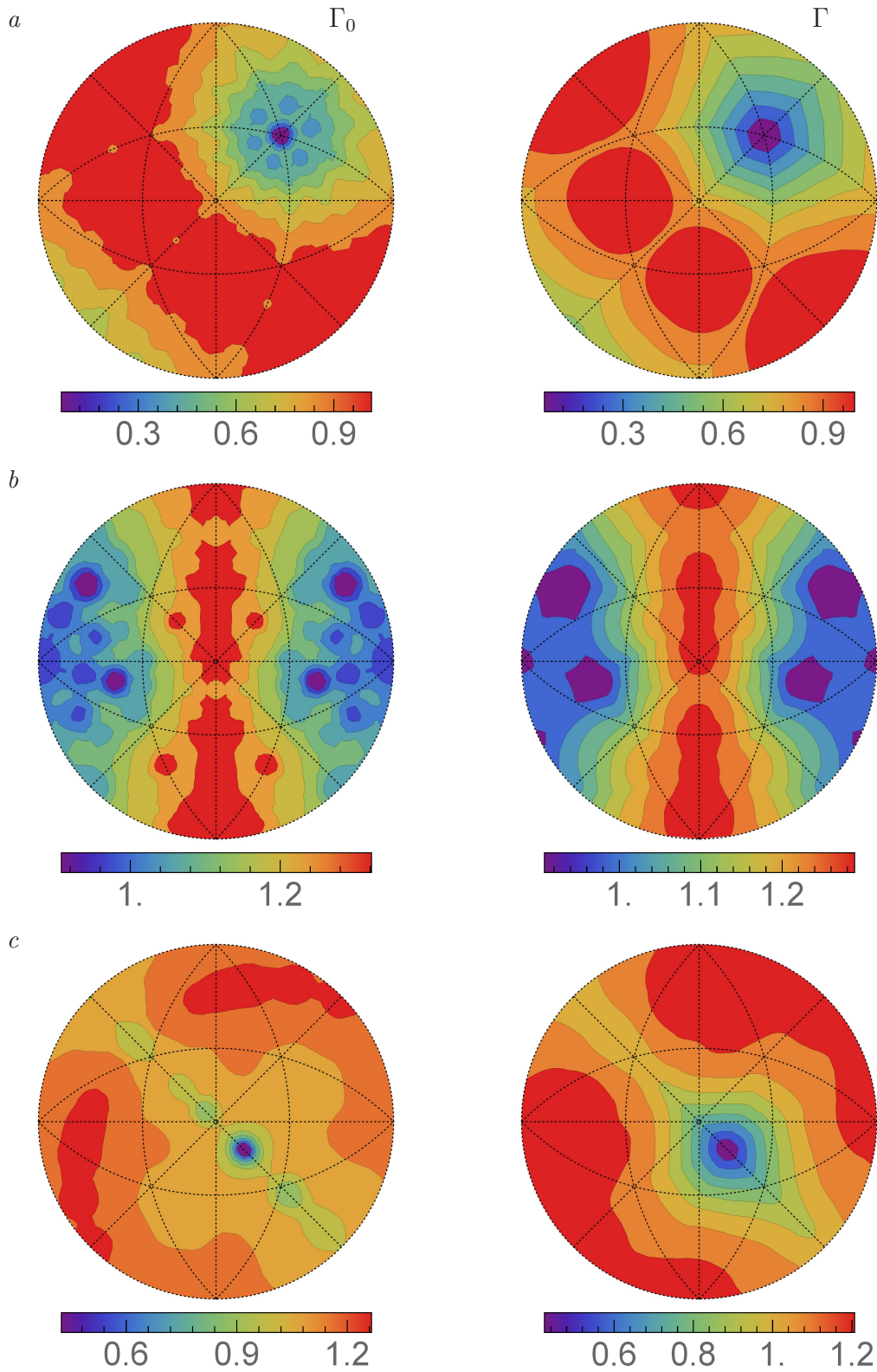


Figure 6: Energy represented by the interpolating function Γ_0 (left column) and h-convex function Γ (right column) for the misorientations Σ_3 (a), Σ_5 (b) and Σ_{11} (c). The energy unit is J/m^2 .

tion parameters. The dependence of Γ on misorientation, with unjustified oscillations and unphysical behavior near zero-misorientation, reflects the underlying interpolating function; see Fig. 8. The well known deficiencies of the interpolation by inverse distance weighting [31], which are largely eliminated from inclination-dependent sections through Γ , remain visible in misorientation-dependent functions. They could be removed by using a more sophisticated interpolation method. However, the space of macroscopic boundary parameters has high dimension and nontrivial geometry, and one needs to take into account that distributions of data points in the space of macroscopic boundary parameters are usually highly non-uniform. Under these conditions, devising a simple but effective interpolation method is challenging.

The resulting h-convex energy function Γ is similar but not the same as that of Bulatov et al. [7]; cf. right columns of Figs. 1 and 6. These two functions are based on different principles. First, the function Γ is computed without assumptions about locations of energy cusps, whereas that of Bulatov et al. [7] is based on presupposed locations of cusps. Second, Γ is computed without assumptions about profiles of the cusps, whereas Bulatov et al. [7] use the RSW function. Third, the number of parameters governing determination of Γ is small (u and N_P plus the choice of the distance function), whereas some forty parameters are used in [7]. Finally, Γ satisfies Herring's condition, whereas the function described in [7] does not (but could serve as Γ_0). On the other hand, due to the use of a simplistic interpolation method, the function Γ shows unphysical features in the energy-misorientation dependence.

As for the computational cost of the described procedure, by far the most expensive part of acquiring data for plots like those in Fig. 6 is the interpolation. It takes over 99% of the total computation time. The cost of interpolation is proportional to $N_P K N_s^2$, where N_s is the number of used crystal symmetry operations. In the considered example (with $N_s = 24$), sequential processing on a 2.6 GHz personal computer took about six minutes per misorientation. In the case of Fig. 8, each point on the abscissa corresponds to a different misorientation. Therefore, obtaining a single point of the one-dimensional color plot in Fig. 8 takes nearly the same time as obtaining all points for one of the two-dimensional plots in Fig. 6.

5 Concluding remarks

The paper addresses the issue of proper modeling of grain boundary energy as a function of macroscopic boundary parameters. Energies represented by the function are assumed to correspond to boundary equilibrium states. For arbitrary constant misorientation, the function

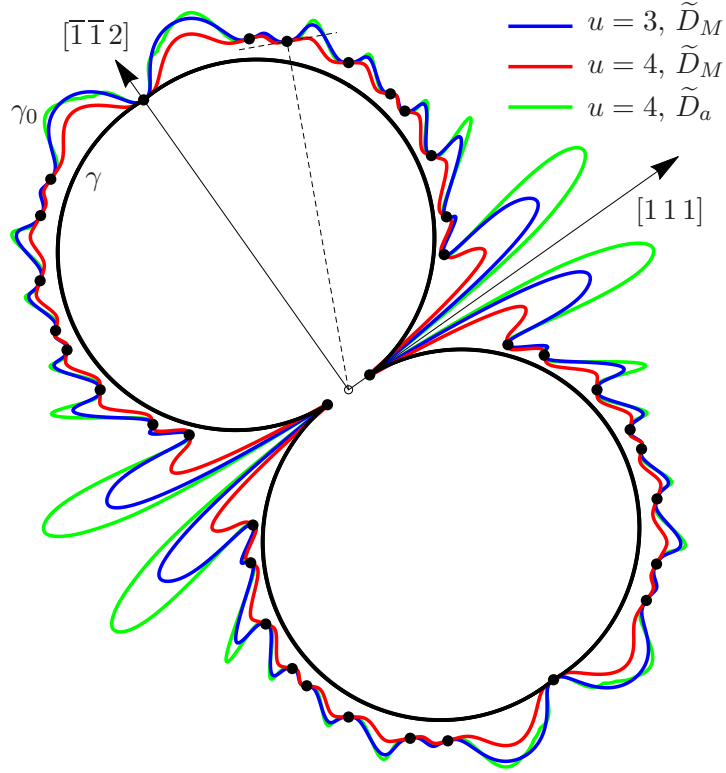


Figure 7: Section perpendicular to $[1\bar{1}0]$ through Wulff plots of the interpolating functions γ_0 and h-convex γ for Σ_3 . The plots are for $u = 3$ and $u = 4$ and for the distances \tilde{D}_a and \tilde{D}_M . H-convexification of functions γ_0 leads to nearly identical resulting functions γ ; they are all shown in black. Disks mark data points from [20]. The magnitude of vectors is 1 J/m^2 .

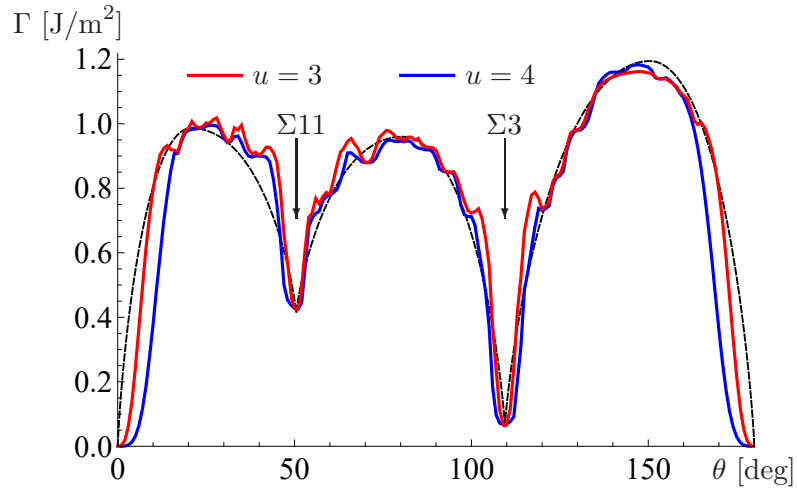


Figure 8: H-convex Γ function for $[110]$ symmetric tilt boundaries versus the tilt angle θ . The interpolating functions Γ_0 (not shown) were computed with $u = 3$ (red graph) and $u = 4$ (blue graph). Dashed black line represents the function described in [7].

should satisfy the condition that the $1/\gamma$ -plot is convex. This property of a global boundary energy function is referred to as h-convexity. It is pointed out that current accounts on determination of boundary energy functions ignore the requirement of h-convexity. Moreover, it is shown that if energy cusps at fixed misorientation are modeled using Read-Shockley-Wolf function, the h-convexity condition is violated.

A function that approximates the true energy function but violates the h-convexity condition can be ‘h-convexified’ by simply replacing all high function values causing the violation by smaller (but the largest possible) values with which the condition is satisfied. The function resulting from the h-convexification may have features expected for an energy function, even if the input function lacks them. In particular, the h-convexification may lead to the appearance of singularities not present in the input function.

The paper provides details of an example procedure for constructing continuous h-convex function based on a discrete dataset of energies. The emphasis is on simplicity. The procedure comes down to h-convexification of a function obtained by Shepard’s interpolation and is governed by a small number of parameters. It does not involve a priori selected locations of singularities and does not use any extrinsic cusp models. Application of the procedure to simulated data of Olmsted et al. [20] leads to a global function similar to that of Bulatov et al. [7], but it requires much fewer assumptions and parameters. Clearly, the nature of the data source is irrelevant, and the procedure can be applied to other types of data, e.g., experimental results or combinations of data from different sources.

The described approach can be seen as a step towards more advanced strategies for modeling of grain boundary energy. Various improvements can be envisioned, but the key issue is to develop a better interpolation method. With an appropriate interpolation scheme, energy singularities in the domain of misorientations (other than that at zero misorientation) could be linked to singularities arising in the domain of plane inclinations (due to vertices and edges of $1/\gamma$ -plots). A properly chosen modeling strategy would allow for avoiding assumptions about locations of singularities.

One might also consider adding the condition that would prevent a configuration to achieve lower energy by replacing a single grain boundary with two or more boundaries parallel to it. In other words, energy of a boundary needs to be lower than the sum energies of any possible replacements. If the energy distribution is close to uniform, the condition is satisfied, but theoretically, a general energy function may violate it.

References

- [1] D.M. Saylor, A. Morawiec, and G.S. Rohrer. Distribution and energies of grain boundaries in magnesia as a function of five degrees of freedom. *J. Amer. Ceram. Soc.*, 85:3081–3083, 2002.
- [2] J. Li, S.J. Dillon, and G.S. Rohrer. Relative grain boundary area and energy distributions in nickel. *Acta Mater.*, 57:4304–4311, 2009.
- [3] H. Beladi, N.T. Nuhfer, and G.S. Rohrer. The five-parameter grain boundary character and energy distributions of a fully austenitic high-manganese steel using three dimensional data. *Acta Mater.*, 70:281–289, 2014.
- [4] Y.F. Shen, X. Zhong, H. Liu, R.M. Suter, A. Morawiec, and G.S. Rohrer. Determining grain boundary energies from triple junction geometries without discretizing the five-parameter space. *Acta Mater.*, 166:126–134, 2019.
- [5] H.K. Kim, W.S. Ko, H.J. Lee, S.G. Kim, and B.J. Lee. An identification scheme of grain boundaries and construction of a grain boundary energy database. *Scripta Mater.*, 64:1152–1155, 2011.
- [6] S.E. Restrepo, S.T. Giraldo, and B.J. Thijsse. Using artificial neural networks to predict grain boundary energies. *Comp. Mater. Sci.*, 86:170–173, 2014.
- [7] V.V. Bulatov, B.W. Reed, and M. Kumar. Grain boundary energy function for fcc metals. *Acta Mater.*, 65:161–175, 2014.
- [8] H. Dette, J. Gösmann, C. Greiff, and R. Janisch. Efficient sampling in materials simulation-exploring the parameter space of grain boundaries. *Acta Mater.*, 125:145–155, 2017.
- [9] R. Sarochawikasit, C. Wang, P. Kumam, H. Beladi, T. Okita, G.S. Rohrer, and S. Ratanaphan. Grain boundary energy function for α iron. *Materialia*, 19:101186, 2021.
- [10] Y. Zhang, E.D. Hansen, T. Harbison, S. Masengale, J. French, and L. Aagesen. A molecular dynamics survey of grain boundary energy in uranium dioxide and cerium dioxide. *J. Am. Ceram. Soc.*, 105:4471–4486, 2022.

- [11] O. Chirayutthanasak, R. Sarochawikasit, A. Wisitsorasak, N. Rujisamphan, T. Frolov, T. Ooppelstrup, S. Dangtip, G.S. Rohrer, and S. Ratanaphan. Anisotropic grain boundary area and energy distributions in tungsten. *Scripta Mater.*, 209:114384, 2022.
- [12] O. Chirayutthanasak, R. Sarochawikasit, S. Khongpia, T. Okita, S. Dangtip, G.S. Rohrer, and S. Ratanaphan. Universal function for grain boundary energies in bcc metals. *Scripta Mater.*, 240:115821, 2024.
- [13] S.G. Baird, E.R. Homer, D.T. Fullwood, and O.K. Johnson. Five degree-of-freedom property interpolation of arbitrary grain boundaries via Voronoi fundamental zone framework. *Comp. Mater. Sci.*, 200:110756, 2021.
- [14] E.R. Homer, G.L.W. Hart, C.B. Owens, D.M. Hensley, J.C. Spendlove, and L.H. Serafin. Examination of computed aluminum grain boundary structures and energies that span the 5D space of crystallographic character. *Acta Mater.*, 234:118006, 2022.
- [15] H.K. Kim, S.G. Kim, W. Dong, I. Steinbach, and B.J. Lee. Phase-field modeling for 3D grain growth based on a grain boundary energy database. *Model. Simul. Mater. Sc.*, 22:034004, 2014.
- [16] H. Hallberg and V.V. Bulatov. Modeling of grain growth under fully anisotropic grain boundary energy. *Model. Simul. Mater. Sc.*, 27:045002, 2019.
- [17] J.D. Niño and O.K. Johnson. Influence of grain boundary energy anisotropy on the evolution of grain boundary network structure during 3D anisotropic grain growth. *Comp. Mater. Sci.*, 217:111879, 2023.
- [18] J. Niño and O.K. Johnson. Evolution of crystallographic texture and grain boundary network structure during anisotropic grain growth. *Comp. Mater. Sci.*, 240:113023, 2024.
- [19] C. Herring. Some theorems on the free energies of crystal surfaces. *Phys. Rev.*, 82:87, 1951.
- [20] D.L. Olmsted, S.M. Foiles, and E.A. Holm. Survey of computed grain boundary properties in face-centered cubic metals: I. Grain boundary energy. *Acta Mater.*, 57:3694–3703, 2009.
- [21] D. Wolf. A Read-Shockley model for high-angle grain boundaries. *Scripta Metall.*, 23:1713–1718, 1989.

- [22] K. Głowiński. *Methods for quantitative characterization of three-dimensional grain boundary networks in polycrystalline materials*. PhD thesis, Polish Academy of Sciences, Institute of Metallurgy and Materials Science, 2015.
- [23] F.C. Frank. The geometrical thermodynamics of surfaces. In N.A. Gjostein and W.D. Robertson, editors, *Metal Surfaces: Structure, Energetics and Kinetics*, ASM Seminar Series, pages 1–15, Metals Park, Ohio, 1963. American Society for Metals.
- [24] A. Morawiec. Symmetries of grain boundary distributions. In B. Adams, A. Rollett, and H. Weiland, editors, *Grain Growth in Polycrystalline Materials III*, pages 509–514, Warrendale, PA, US, 1998. TMS.
- [25] A. Morawiec. Models of uniformity for grain boundary distributions. *J. Appl. Cryst.*, 42:783–792, 2009.
- [26] C. Rottman and M. Wortis. Statistical mechanics of equilibrium crystal shapes: Interfacial phase diagrams and phase transitions. *Phys. Rep.*, 103:59–79, 1984.
- [27] T.E. Hsieh and R.W. Balluffi. Observations of roughening/de-faceting phase transitions in grain boundaries. *Acta Metall.*, 37:2133–2139, 1989.
- [28] A. Brokman, P.D. Bristowe, and R.W. Balluffi. Atomistic faceting of asymmetric tilt boundaries. *Scripta Metall.*, 15:201–206, 1981.
- [29] W.T. Read and W. Shockley. Dislocation models of crystal grain boundaries. *Phys. Rev.*, 78:275–289, 1950.
- [30] J. O’Rourke. *Computational geometry in C*. Cambridge University Press, Cambridge, UK, 1998.
- [31] D. Shepard. A two-dimensional interpolation function for irregularly-spaced data. In *Proceedings of the 1968 23rd ACM National Conference*, pages 517–524, 1968.
- [32] A. Morawiec. On distances between grain interfaces in macroscopic parameter space. *Acta Mater.*, 181:399–407, 2019.
- [33] J. O’Rourke. `chull.c` on GitHub: <https://github.com/OSGeo/grass/blob/main/vector/v.hull/chull.c>. Accessed: 2024-06-11.
- [34] A. Morawiec. A new metric for the space of macroscopic parameters of grain interfaces. *Metall. Mater. Trans. A*, 50:4012–4015, 2019.